J Mol Model (2017) 23: 89
DOI 10.1007/s00894-017-3244-9

ORIGINAL PAPER

Polaron stability in oligoacene crystals

Marcelo Lopes Pereira Junior[1] · **Luiz Antonio Ribeiro Junior**[2]

Received: 5 October 2016 / Accepted: 23 January 2017 / Published online: 22 February 2017

Abstract The polaron stability in organic molecular crystals is theoretically investigated in the scope of a two-dimensional Holstein–Peierls model that includes lattice relaxation. Particularly, the investigation is focused on designing a model Hamiltonian that can address properly the polaron properties in different model oligoacene crystals. The findings showed that a suitable choice for a set of parameters can play the role of distinguishing the model crystals and, consequently, different properties related to the polaron stability in these systems are observed. Importantly, the usefulness of this model is stressed by investigating the electronic localization of the polaron, which provides a deeper understanding into the properties associated with the polaron stability in oligoacene crystals.

Keywords Polaron stability · Organic semiconductors · Oligoacenes · Molecular crystals

This paper belongs to Topical Collection VI Symposium on Electronic Structure and Molecular Dynamics – VI SeedMol

✉ Luiz Antonio Ribeiro Junior
ribeirojr@unb.br

Marcelo Lopes Pereira Junior
marcelolpjunior@gmail.com

[1] University of Brasília, Campus Planaltina, PPG-CIMA, 73345-010, Brasília, DF, Brazil

[2] International Center for Condensed Matter Physics, University of Brasília, PO Box 04531, 70.919-970 Brasília, DF, Brazil

Introduction

Organic molecular crystals have attracted much attention since the discovery of their charge transport properties [1, 2]. Unique traits, such as low cost, light weight, and flexibility make them interesting for the electronics industry, particularly when it comes to promising solutions for new green energy applications [3, 4]. Since charge transport is the key step behind the performance of organic-based optoelectronic devices such as OPVs [5] and OLEDs [6], a more detailed understanding about the polaron stability features at a molecular scale is fundamental.

The oligoacenes compose a class of materials largely used in the field of organic electronics [1]. Particularly, tetracene [7], pentacene [8], and derivatives [9] have been employed in developing organic devices mostly for presenting well-defined crystal structures. Other types of oligoacenes such as naphthalene, anthracene, and rubrene have been also used for designing optoelectronic devices in several recent studies [10–14]. These materials exhibit two types of electron-lattice interactions, the local intramolecular (Holstein-type) and non-local intermolecular (Peierls-type), presenting weak intermolecular van der Waals bonds [12]. In this way, to account for these two types of electron-lattice vibrations, the Holstein and Peierls approaches should be incorporated into a single model Hamiltonian, named Holstein–Peierls Hamiltonian [10]. Several studies addressed the polaron dynamics in oligoacene crystals by employing the Holstein–Peierls model [15–21]. Nonetheless, studies concerning the polaron stability in the materials are very few in the literature, which requires further investigations.

In this work, a systematic numerical study is performed to investigate the polaron stability in different oligoacene crystals using a semi-empirical Holstein–Peierls model. The computational protocol is based on defining model parameters that resemble single layers of the following oligoacene crystals: napthtalene, anthracene, pentacene, tetracene, and rubrene. Importantly, the results presented here may throw new light on the description of the polaron properties in oligoacene crystals.

Methodology

The model Hamiltonian adopted here considers both intra and intermolecular electron-lattice interactions for describing a two-dimensional array (single layer) of N molecules. Each molecule in the array is defined as a site i,j with three degrees of freedom: two antisymmetric non-local $v_x^{i,j}$ and $v_y^{i,j}$ phonon modes and one local phonon mode u_i, as represented in Fig. 1. In this molecular array, the index i (x-direction) denotes the "rows" whereas j (y-direction) labels the "columns".

The model Hamiltonian that incorporates the Holstein [22, 23] and Peierls [17, 24–27] approaches in a single Hamiltonian and describes the molecular array can be expressed as

$$H = H_{elec,1} + H_{elec,2} + H_{latt,1} + H_{latt,2} \tag{1}$$

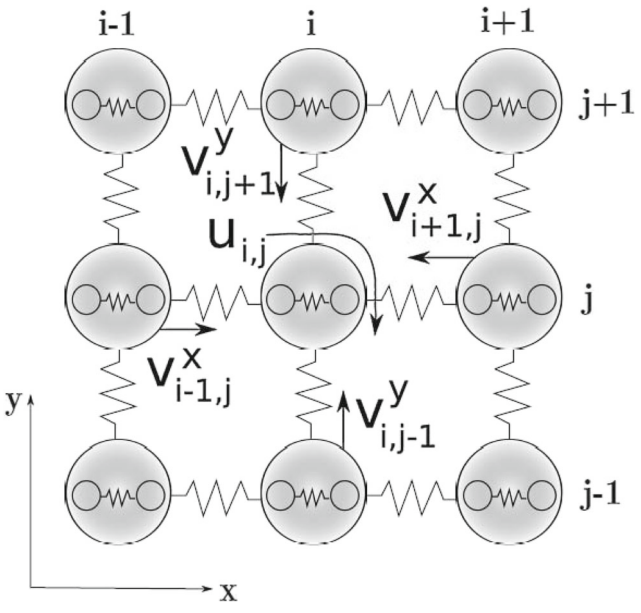

Fig. 1 Schematic representation of the molecular array adopted here. $v^x_{i,j}$ and $v^y_{i,j}$ are the intermolecular displacements of a molecule in x- and y-direction, respectively, whereas u_i is the internal displacement of a given molecule

with

$$H_{elec,1} = \sum_{i,j} \alpha_1 u_{i,j} \hat{c}^{\dagger}_{i,j} \hat{c}_{i,j} \tag{2}$$

and

$$H_{elec,2} = \sum_{i,j} (J^x_{i+1,j,i,j} \hat{c}^{\dagger}_{i,j} \hat{c}_{i+1,j} + h.c.) + \sum_{i,j} (J^y_{i,j+1,i,j} \hat{c}^{\dagger}_{i,j+1} \hat{c}_{i,j} + h.c.). \tag{3}$$

The indexes 1 and 2 refer to Holstein and Peierls contributions, respectively. $H_{elec,1}$ and $H_{elec,2}$ describe the electronic part of the model Hamiltonian. The operator $\hat{c}^{\dagger}_{i,j}$ ($\hat{c}_{i+1,j}$) creates (annihilates) a carrier at the (i, j)-th molecule, α_1 is the intramolecular electron-phonon (e-ph) coupling, $J^{x,y}_{i,j,i',j'}$ are the transfer integrals that consider the intermolecular interactions and have the following form

$$J^x_{i+1,j,i,j} = J^x_0 - \alpha^x_2 (v^x_{i+1,j} - v^x_{i,j}) \tag{4}$$

and

$$J^y_{i,j+1,i,j} = J^y_0 - \alpha^y_2 (v^y_{i+1,j} - v^y_{i,j}). \tag{5}$$

$H_{latt,1}$ and $H_{latt,2}$ describe the lattice backbone using two isolated harmonic oscillators for the intra and intermolecular phonon modes:

$$H_{latt,1} = \frac{K_1}{2} \sum_{i,j} (u_{i,j})^2 + \frac{M_1}{2} \sum_{i,j} (\dot{u}_{i,j})^2 \tag{6}$$

and

$$H_{latt,2} = \frac{K_2}{2} \sum_{i,j} \left[(v^x_{i+1,j} - v^x_{i,j})^2 + (v^y_{i,j+1} - v^y_{i,j})^2 \right] + \frac{M_2}{2} \sum_{i,j} \left[(\dot{v}^x_{i,j})^2 + (\dot{v}^y_{i,j})^2 \right], \tag{7}$$

where K_1 (K_2) and M_1 (M_2) are the force constant and molecular mass for the intramolecular (intermolecular) phonon mode, respectively.

The main focus of the present study is to investigate the possible differences for the polaron stability in some oligoacene crystals using a parametrized model Hamiltonian. In order to do so, the intermolecular (Peierls) parameters α_2 and K_2 vary systematically in the intervals [0.1–2.0] eV/Å and [1–10] eV/Å^2, respectively. The increment for α_2 is defined to be 0.1 eV/Å whereas for K_1 the increment is 1.0 eV/Å^2. The other remaining parameters are settled as presented in Table 1. It is worthwhile to mention that the values for the transfer integrals $J^{x,y}_0$ were used successfully in other theoretical studies [10, 11, 19–21, 28–34] whereas the values for α_1 and K_1 were obtained in calculations performed here. In these calculations, the values for α_1 and K_1 have been chosen in order to obtain the minimal

Table 1 Set of parameters used in the simulations

System	M_1 [eV(as/Å)^2]	M_2 [eV(as/Å)^2]	$J_0^{x,y}$ [meV]	α_1 [eV/Å]	K_1 [eV/Å^2]
Naphthalene	1.30×10^9	2.60×10^{10}	35.6	0.63	4.18
Anthracene	1.84×10^9	3.68×10^{10}	44.9	0.79	5.27
Pentacene	2.88×10^9	5.76×10^{10}	85.2	1.50	10.00
Tetracene	2.36×10^9	4.72×10^{10}	69.5	1.22	8.16
Rubrene	5.52×10^9	1.10×10^{11}	105	1.85	12.32

values necessary to the appearance of stable polarons for $\alpha_2 = 0.5$ eV/Å and $K_2 = 1.5$ eV/Å, which are recognized as standard for modeling organic crystals in the scope of the Holstein–Peierls model [10, 12, 20, 27].

Results

In our calculations for the polaron stability, the ground state geometry is optimized using the resilient backpropagation (RPROP) algorithm [35]. From these calculations, we obtain the distortions associated to the absence/presence of an electron, the molecular charge localization and, consequently, the total energy of the system. The systems are formed by a two-dimensional (20×20) molecular array with periodic boundary conditions using the parameters given in the previous section for each model oligoacene crystal. It is well known that adding/removing an electron to/from an unsaturated organic material leads to deformations in the lattice. The mutual interaction between the electron or hole with these deformations results in a quasiparticle that is composed of a charge surrounded by a cloud of phonons. This resulting quasiparticle is named Polaron [12]. The above-mentioned interaction between charge and lattice costs to the system an extra energy that can be related to the polaron's presence in the model crystal.

The polaron formation energy (E_P) represents the difference between the energies for systems in the neutral ground state and in a relaxed configuration due to the presence of an extra electron or hole [12]. For stable polarons, $E_P > 0$ and can be expressed as

$$E_P = 2(J_0^x + J_0^y) - E_{\pm} \tag{8}$$

according to reference [12], where $E_{\pm}$ states the system total energy for an added hole or electron. E_P values much higher than $J_0^{x,y}$ indicate that the polaron is localized mostly in a single molecular unit (small polaron) whereas for $E_p \sim J_0^{x,y}$ the polaron extends over several units (large polaron).

With this knowledge about the polaron formation in organic semiconductors in mind, we can now discuss the resulting polaron formation energies in the model oligoacene crystals investigated here. In this way, Fig. 2 presents E_P as a function of α_2 and K_2 for the pentacene system. It is worthwhile to mention that the interplay between E_P and the Peierls parameters presents, qualitatively, the same trend for the other systems, i.e., E_P increases substantially for small K_2 and high α_2 values, as can be seen in Fig. 2. From this figure, it is also possible to note that there is a boundary (green region) between the planar grey and the sharp red regions. The grey region indicates the parameter space in which the ground state solution is a large polaron. In this region, the polaron formation energies lie in the range of 0.4–0.8 eV. The red regions, in turn, point to the parameter space in which the geometry optimization procedure leads to small polaron solutions. The green region defines the parameter space for transient structures between large and small polarons. It worth to stress here that some values for E_P, mostly in green and red regions of Fig. 2, are unrealistic high and are not interesting in the context of semiconducting molecular crystals for which E_P is smaller than 0.5 eV [12, 31, 32]. Moreover, the charge carriers in organic crystals are commonly large polarons [12]. The energy range for E_P concerning the other model crystals simulated here are: 0.28–4.15 eV for napthtalene, 0.36–4.20 eV for anthracene, 0.4–4.30 eV for pentacene, 0.56–4.5 eV for tetracene, and 0.84–4.60 eV for rubrene. Importantly, E_P tends to increase when $J_0^{x,y}$ is increased, as can be inferred from Eq. 8. From Fig. 2 it is also possible to conclude that the parameter space for α_2 and K_2 that leads to small polaron solutions is quite limited. This is clear evidence that the combined Holstein–Peierls model leads naturally to stable large polaron solutions and that it is a suitable approach to study the formation of polarons in organic molecular crystals.

The differences between E_P for the oligoacenes adopted here can be better understood by examining Fig. 3. This figure presents E_P as a function of K_2 for all model crystals simulated here considering $\alpha_2 = 0.5$ eV/Å that, as mentioned before, was adopted in other theoretical studies as a standard value for one of the Peierls parameters. From this figure, one can see that E_P decreases when K_2 is increased. Despite the difference among the E_P values, the interplay between E_P and K_2 presents the same trend for all systems. Moreover, Fig. 3 clearly shows that the most important parameter to define the polaron formation energy is the molecular transfer integral, once model crystals with higher J_0 present higher E_P. In other words, the electronic

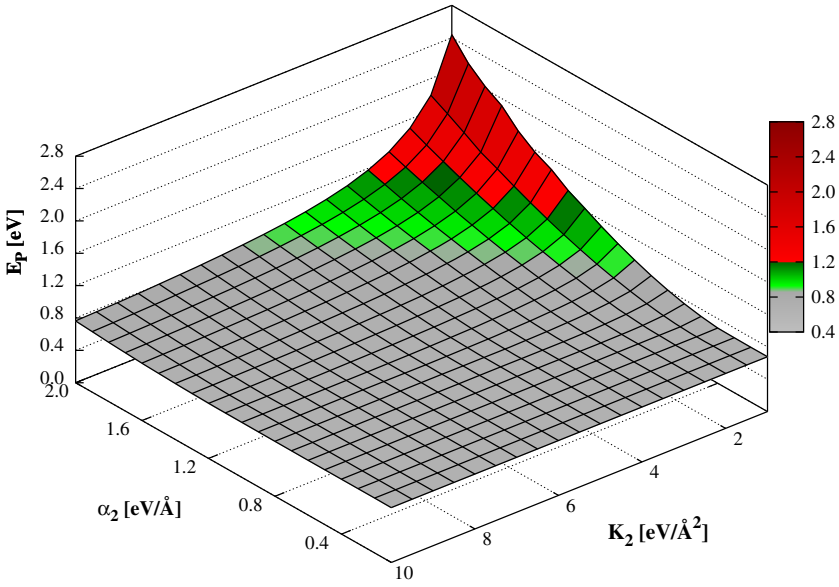

Fig. 2 Polaron formation energy (E_P) for the pentacene system as a function of Peierls parameters α_2 and K_2. The *grey region* indicates the parameter space for large polaron solutions whereas the *red regions* show the parameter space for small polaron solutions

energy is dominant in defining the polaron formation energy in oligoacene crystals.

Now we turn to the geometry configuration and the molecular charge localization associated to the presence of a hole-polaron (absence of an electron) in the system. Figure 4 presents the standard ground state configuration for (a) molecular charge density, (b) intramolecular displacement $u_{i,j}$, (c) intermolecular displacement in the x-direction $v^x_{i+1,j} - v^x_{i,j}$, and (d) intermolecular displacement in the y-direction $v^y_{i,j+1} - v^y_{i,j}$ of a large polaron in a 20×20 pentacene system. For the sake of comparison with other theoretical predictions, in this case $\alpha_2 = 0.5$ eV/Å and $K_2 = 1.5$ eV/Å^2. In this way, from Fig. 4a one can see that the polaron is localized essentially in five molecular units and the main portion of the charge lies in a central unity. The other remaining molecules that contain charge are the next-neighboring ones in x and y directions. This arrangement shows that the polaron structure has a two-dimensional nature in organic crystals. A similar trend is presented for distortions of the internal coordinate $u_{i,j}$, as shown in Fig. 4b. From this figure one can realize that the distortions associated with the presence of charge show negative values that represent a compression of the molecules. The other molecules in the model crystal present $u_{i,j} = 0$, which states that there is no charge localized in these sites. The intermolecular displacements, in turn, present a contraction (negative distortions) for the next-neighboring displacements around the central unity in x and y directions, as shown in Fig. 4c and d, respectively. These contractions cause lattice expansions (positive distortions) in x and y directions through the row and column of the molecular array where the central unity is placed. For larger crystals, at least 50×50, the expansions decrease by a factor of $\delta/n_{x,y}$, where δ is the value for the first positive displacement and $n_{x,y}$ the total number of molecules in one of the directions. This process occurs in order to keep the constraint of fixed total displacement,

$$\sum_i v^x_{i+1,j} - v^x_{i,j} = \sum_j v^y_{i,j+1} - v^y_{i,j} = 0. \quad (9)$$

It is worth highlighting that the configurations for the molecular charge and lattice displacements discussed above are qualitatively similar for the other model oligoacene crystals considered here. Moreover, even considering other different parameters, the overall shape for the molecular

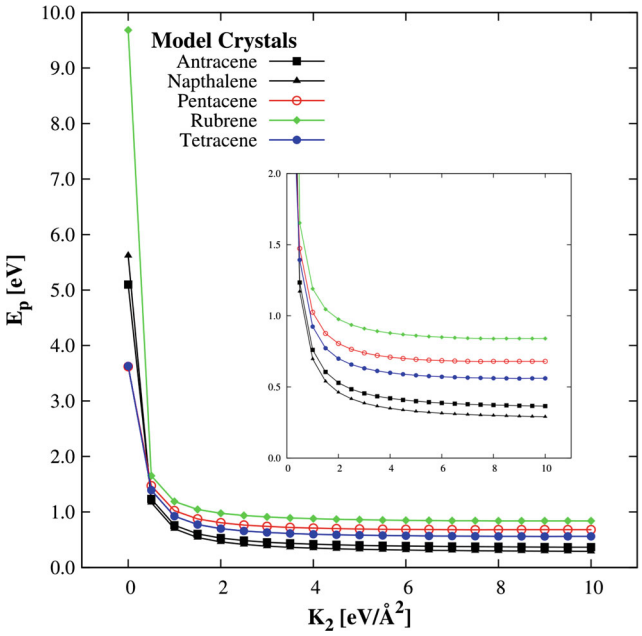

Fig. 3 Comparison between the polaron formation energies obtained for all model crystals considering $\alpha_2 = 0.5$ eV/Å

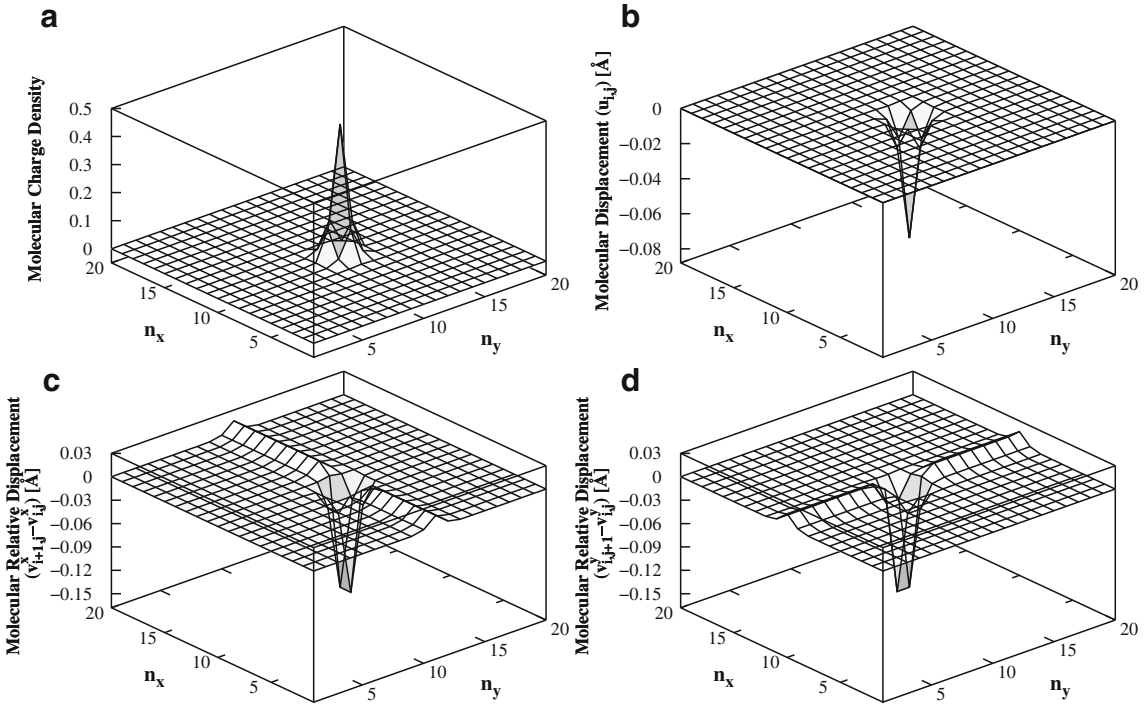

Fig. 4 Standard ground state configuration for **a** molecular charge density, **b** intramolecular displacement, **c** intermolecular displacement in x-direction, and **d** intermolecular displacement in y-direction of a 20 × 20 pentacene system

charge distribution and lattice deformations for the pentacene crystal are qualitatively similar to the ones reported in references [19, 20].

Finally, in order to better clarify the differences between the polaron properties in the model oligoacene crystals, we now discuss the electronic localization for the polaron. Here, this is accomplished by analyzing the inverse participation ratio (IPR) concerning the charge density

$$IPR = \frac{\sum_i |\psi_{i,j}|^4}{\left(\sum_i |\psi_{i,j}|^2\right)^2}, \tag{10}$$

which is calculated using the molecular charge distribution for the ground state configuration. Primarily, the IPR value indicates the assignments for the polaron localization. For values higher than 0.7, the carrier is localized basically in a single molecule, which renders a structure named small polaron. IPR values spanning from 0.3 to 0.7 denote a large polaron solution in which the molecular charge is distributed among more than three crystal's constituents being the most part of the charge shared between one or two central unities. For these IPR values, the polaron is stable. Conversely, IPR values smaller than 0.3 point to cases where there is no polaron formation (delocalized states).

With the information about the relationship between IPR and polaron localization in mind, we can now discuss the electronic properties of the polaron in different oligoacene crystals. Table 2 displays the IPR values obtained for the oligoacene systems considered here. The first evidence presented by this table is that a large polaron solution can be obtained in all model crystals, since the lowest IPR value is higher than 0.37. Moreover, from Table 2 it is possible to conclude that the higher the system's transfer integral the lower is the IPR. The results presented in Table 2 can be better understood by noticing the nature for the electronic part of our model (see Eqs. 4 and 5), which are based in a hopping term J_0 between next-neighboring molecules. For larger $J_0^{x,y}$, the greater the probability of an electronic transference between next-neighboring units and, consequently, the polaronic charge becomes even more delocalized. It is worthwhile to mention that the polaron localization also depends on the interplay between the transfer integral and the electron-phonon coupling strength, as reported in reference [29].

Table 2 IPR values for the model oligoacene crystals considered in this work

System	IPR
Naphthalene	0.5963
Anthracene	0.5528
Pentacene	0.4707
Tetracene	0.3960
Rubrene	0.3719

Conclusions

In summary, the polaron stability in model oligoacene crystals is numerically studied in the scope of a two-dimensional Holstein–Peierls model that includes electron–phonon interactions. The aim of this work relies on designing a model Hamiltonian that can distinguish between the polaron properties in different oligoacene crystals. The results showed that a suitable set of parameters can play the role of distinguishing the properties related to the polaron stability in these systems. The inverse participation ratio has pointed out to a signature for the localization of the polaronic charge in each model crystal. Moreover, it was also possible to conclude that the parameter space that leads to small polaron solutions is quite limited. The combined Holstein–Peierls model leads naturally to stable large polaron solutions, proving to be a suitable approach to study the formation of polarons in organic molecular crystals, since charge carriers in organic crystals are commonly large polarons.

Acknowledgments The authors gratefully acknowledge the financial support from the Brazilian Research Councils CNPq, CAPES, and FINATEC. L.A.R.J. gratefully acknowledges the financial support from the Brazilian Research Council FAPDF grant 0193.000942/2015. L.A.R.J. also wishes to thank the Brazilian Ministry of Planning, Budget and Management (Grant DIPLA 005/2016).

References

1. Coropceanu V, Cornil J, da Silva Filho DA, Olivier Y, Silbey R, Brédas JL (2007) Chem Rev 107:926. doi:10.1021/cr050140x
2. Karl N (2003) Synth Metals 133:649. doi:10.1016/S0379-6779(02)00398-3
3. Deotare PB, Chang W, Hontz E, Congreve DN, Shi L, Reusswig PD, Modtland B, Bahlke ME, Lee CK, Willard AP, Bulovic V, Van Voorhis T, Baldo MA (2015) Nanoscale transport of charge-transfer states in organic donor-acceptor blends. Nat Mat 14:1130. doi:10.1038/nmat4424
4. Zhang Q, Sun Y, Xu W, Zhu D (2014) Organic thermoelectric materials: emerging green energy materials converting heat to electricity directly and efficiently. Adv Mat 26:6829. doi:10.1002/adma.201305371
5. Vandewal K, Albrecht S, Hoke ET, Graham KR, Widmer J, Douglas JD, Schubert M, Mateker WR, Bloking JT, Burkhard GF, Sellinger A, Fréchet JMJ, Amassian A, Riede MK, McGehee MD, Neher D, Salleo A (2014) Nat Mat 13:63. doi:10.1038/nmat3807
6. White MS, Kaltenbrunner M, Gowacki ED, Gutnichenko K, Kettlgruber G, Graz I, Aazou S, Ulbricht C, Egbe DAM, Miron MC, Major Z, Scharber MC, Sekitani T, Some T, Bauer S, Sariciftci NS (2013) Nat Phot 7:811. doi:10.1038/nphoton.2013.188
7. Salman S, Delgado MCR, Coropceanu V, Brédas JL (2009) Chem Mater 21(15):3593. doi:10.1021/cm901128j
8. Lucas B, Amranib AE, Molitona A, Skaikya A, Hajja AE, Aldissic M (2012) Solid-State Elec 69:99. doi:10.1016/j.sse.2011.12.011
9. McGarry KA, Xie W, Sutton C, Risko C, Wu Y, Young VG, Brédas JL, Frisbie CD, Douglas CJ (2013) Chem Mater 25(11):2254. doi:10.1021/cm400736s
10. Troisi A (2011) Chem Soc Rev 40:2347. doi:10.1039/c0cs00198h
11. Troisi A (2011) J Chem Phys 134:034702. doi:10.1063/1.3524314
12. Stafström S (2010) Chem Soc Rev 39:2484. doi:10.1039/b909058b
13. Shuai Z, Wang L, Li Q (2011) Adv Mater 23:1145. doi:10.1002/adma.201003503
14. Arago J, Troisi A (2016) Adv Func Mat 26:2316. doi:10.1002/adfm.201503888
15. Kalosakas G, Aubry S, Tsironis GP (1998) Phys Rev B 58:3094. doi:10.1103/PhysRevB.58.3094
16. Hannewald K, Bobbert PA (2004) Appl Phys Lett 85:1535. doi:10.1063/1.1776335
17. Ortmann F, Bechstedt F, Hannewald K (2009) Phys Rev B 79:235206. doi:10.1103/PhysRevB.79.235206
18. Hannewald K, Stojanović VM, Schellekens JMT, Bobbert PA, Kresse G, Hafner J (2004) Phys Rev B 69:075211. doi:10.1103/PhysRevB.69.075211
19. Mozafari E, Stafström S (2012) Phys Lett A 376:1807. doi:10.1016/j.physleta.2012.04.007
20. Mozafari E, Stafström S (2013) J Chem Phys 138:184104. doi:10.1063/1.4803691
21. Lee MH, Troisi A (2016) J Chem Phys 144:214106. doi:10.1063/1.4953043
22. Holstein T (1959) Ann Phys 8:325. doi:10.1016/0003-4916(59)90002-8
23. Holstein T (1959) Ann Phys 8:343. doi:10.1016/0003-4916(59)90003-X
24. Emin D, Holstein T (1976) Phys Rev Lett 36:323. doi:10.1103/PhysRevLett.36.323
25. Song L, Shi Q (2015) J Chem Phys 142:174103. doi:10.1063/1.4919061
26. Ishii H, Honma K, Kobayashi N, Hirose K (2012) Phys Rev B 85:245206. doi:10.1103/PhysRevB.85.245206
27. Girlando A, Grisanti L, Masino M, Bilotti I, Brillante A, Valle RGD, Venuti E (2010) Phys Rev B 82:035208. doi:10.1103/PhysRevB.82.035208
28. Junior LAR, Stafström S (2015) Phys Chem Chem Phys 17:8973. doi:10.1039/c4cp06028h
29. Junior LAR, Stafström S (2016) Phys Chem Chem Phys 18:1386. doi:10.1039/c5cp06577a
30. Olivier Y, Lemaur V, Brédas JL, Cornil J (2006) J Phys Chem A 110:6356. doi:10.1021/jp0571933
31. Gruhn NE, da Silva Filho DA, Bill TG, Malagoli M, Coropceanu V, Kahn A, Brédas JL (2002) J Amer Chem Soc 124:7918. doi:10.1021/ja0175892
32. Hultell M, Stafström S (2006) Chem Phys Lett 429:446. doi:10.1016/j.cplett.2006.07.042
33. Sánchez-Carrera RS, Paramonov P, Day GM, Coropceanu V, Brédas JL (2010) J Am Chem Soc 132(41):14437. doi:10.1021/ja1040732
34. Sanchez-Carrera RS, Paramonov P, Day GM, Coropceanu V, Brédas JL (2010) J Amer Chem Soc 132:14437–14446. doi:10.1021/ja1040732
35. Riedmiller M, Braun H (1993) Proceedings of the IEEE International Conference on Neural Networks 1:586. doi:10.1109/ICNN.1993.298623